PROTEINS: Structure, Function, and Genetics 33:265–284 (1998)

Molecular Dynamics Study of Calbindin D_{9k} in the Apo and Singly and Doubly Calcium-Loaded States

Sylvie Marchand and Benoît Roux*
Groupe de Recherche en Transport Membranaire (GRTM), Départements de chimie et physique, Université de Montréal, Montréal, Québec, Canada

ABSTRACT **Molecular dynamics simulations based on detailed atomic models are used to examine the structure and dynamics of calbindin D_{9k}, a protein possessing a pair of EF-hands able to bind two calcium ions in a cooperative fashion. Trajectories for the apo and singly (in the C-terminal binding site) and doubly loaded structures are generated and analyzed. Each system is solvated in a 27 Å radius sphere of 2,285 explicit water molecules. The influence of the remaining bulk is incorporated through a stochastic boundary potential including a solvent reaction field. Long-range electrostatic interactions are treated with a special method and are not truncated. The average structural and dynamic properties upon calcium binding are studied at the atomic level to gain insight into the cooperative interactions between the two binding sites. Results from the trajectories are compared with data from nuclear magnetic resonance (NMR) spectroscopy and X-ray crystallography. NMR ^{15}N and $^{13}C_\alpha$ backbone relaxation order parameters and crystallographic *B*-factors are calculated. Generally, there is a good qualitative agreement between calculated and observed properties. Results confirm that the doubly loaded state is closer, both structurally and dynamically, to the singly loaded state than either of these is to the apo state. It is observed that both hydrogen bonding and the packing of nonpolar side chains contribute to the coupling between the calcium binding sites. Two backbone-to-backbone hydrogen bonds linking the calcium-binding EF-hands (Leu23-O ··· HN-Val61 and Val61-O ··· HN-Leu23) are sensitive to the state of occupancy. Residues Leu23 and Val61 exhibit the smallest rms fluctuations of the entire protein in the D state. In addition, the van der Waals interaction of Val61 with the rest of the protein varies with the calcium-binding state. Proteins 33:265–284, 1998.**

Key words: NMR; order parameters; *B*-factors; EF-hands; hydrogen bonds; hydration; cooperativity

INTRODUCTION

The binding of calcium to specific proteins plays a key role in the regulation of numerous fundamental physiological processes.[1,2] Members of the calmodulin superfamily are a particularly important class of calcium-regulatory proteins, which act as modulators of calcium signaling.[3–6] Several proteins in the calmodulin superfamily, such as calmodulin and troponin C, respond to the binding of calcium by a substantial conformational rearrangement, which is the basis for their regulatory function.[7,8] Other members of the superfamily, such as calbindin D_{9k} (CAB), do not undergo a large conformational change upon calcium binding [the term D_{9k} refers to the synthesis of calbindin, which is controlled by a hormonally active form of vitamin D (1,25-dihydroxyvitamin D_3); the 9k refers to its molecular weight of 8,700 daltons]. CAB is expressed in high prevalence in organs in which calcium transport and uptake occur, e.g., in epithelial cells of the small intestine, in kidney, placenta, uterus, teeth, bone, lung, and growth cartilage. Its main function is to act as a calcium buffer.[9] In addition, CAB appears to aid in calcium uptake from the brush border membrane to the basolateral membrane in the small intestine, as well as transport through placenta and kidney, although the role it plays in these processes remains poorly understood.[9,10]

CAB binds two calcium ions with high affinity; the association constants lie between 2×10^6 and 6×10^8 M^{-1}, depending on the ionic strength.[11,12] Calcium binding occurs in a cooperative fashion, i.e., the binding of a first ion increases the affinity for the binding of a second ion. The free energy of cooperativity has been evaluated at -1.84 kcal/mol at a 50 mM concentration of KCl.[12] The functional unit responsible for cooperativity is a pair of helix-loop-helix calcium-binding supersecondary structure, commonly called EF-hands,[13,14] to which calcium binds with positive cooperativity. Such a pair of EF-hands, which forms the functional unit enabling cooperativ-

Grant sponsor: Medical Research Council.
*Correspondence to: Benoît Roux, Groupe de Recherche en Transport Membranaire (GRTM), Départements de chimie et physique, Université de Montréal, C.P. 6128, succ. Centre ville, Montréal, Québec, Canada H3C 3J7. E-mail: rouxb@plgcn.umontreal.ca
Received 13 February 1998; Accepted 1 June 1998

ity in calcium binding, is a structural motif common to all members of the calmodulin superfamily.[14] Cooperative calcium binding increases the sensitivity to small variations in calcium concentration and, for this reason, is an important factor in the function of the regulatory proteins of the calmodulin superfamily. Thus, understanding the molecular basis of cooperativity is a central question for the function of calcium-regulatory proteins.

CAB represents an attractive model system for investigating the molecular basis of cooperativity in calcium binding. With only 75 amino acids, it is one of the smallest member of the calmodulin superfamily possessing a pair of functional calcium-binding EF-hand.[12,15,16] In addition, the structure of CAB in various calcium-loaded state has been extensively characterized experimentally. The three-dimensional structure of the calcium-bound doubly loaded state was determined using X-ray crystallography.[17–19] The solution structure of the doubly loaded state,[20,21] singly loaded state (with Cd^{2+} in the C-terminal binding site),[22] and apo (calcium-free) state[23] has been determined to high resolution by nuclear magnetic resonance (NMR). Briefly, CAB is composed of a pair of helix-loop-helix EF-hands, connected by a short linker of 10 residues. Two backbone-to-backbone hydrogen bonds between Leu23 and Val61 form a short β-strand structure coupling the calcium-binding EF-hands.[24] A schematic view of the CAB structure in the doubly loaded state is shown in Figure 1.

The structural studies show that CAB does not undergo any major conformational change upon binding either one or two calcium ion(s).[19–23] The rearrangements of the side chains upon calcium binding to the C-terminal EF-hand (site II) do not affect significantly the backbone conformation of the N-terminal EF-hand (site I) and induce only modest structural changes in the nonpolar side chains.[22] Interestingly, NMR backbone ^{15}N relaxation measurements indicate that the binding of one or two calcium ions alters the internal dynamics by reducing the structural fluctuations.[25,26] Using simple mean-field statistical models based on NMR backbone N-H order parameters, it has been suggested that the fluctuations for the different states of occupancy may be interpreted in terms of an entropy of calcium binding.[27] Such a mechanism, based on changes in dynamics rather than structure, differs essentially from classical views of cooperativity in allosteric enzymes.[28,29] A characterization of the system at the molecular level is necessary to further our understanding of the microscopic factors enabling CAB to bind two calcium ions with positive cooperativity.

A powerful approach to address such questions is provided by computer simulations based on detailed atomic models. The goal of the present work is to explore the structural and dynamic properties of the calcium-loaded states of CAB at the microscopic level using molecular dynamics simulations. CAB is an ideal model system for computational studies of calcium binding cooperativity at the microscopic level. It is relatively small (75 amino acids) and amenable to calculations that are not prohibitively expensive. Furthermore, the absence of large conformational changes upon calcium binding is computationally advantageous. Trajectories of atomic models of the apo (calcium-free), singly loaded with a calcium in site II, and doubly loaded states were generated and analyzed. The trajectories were initiated from the available experimentally determined high-resolution X-ray and NMR structures.

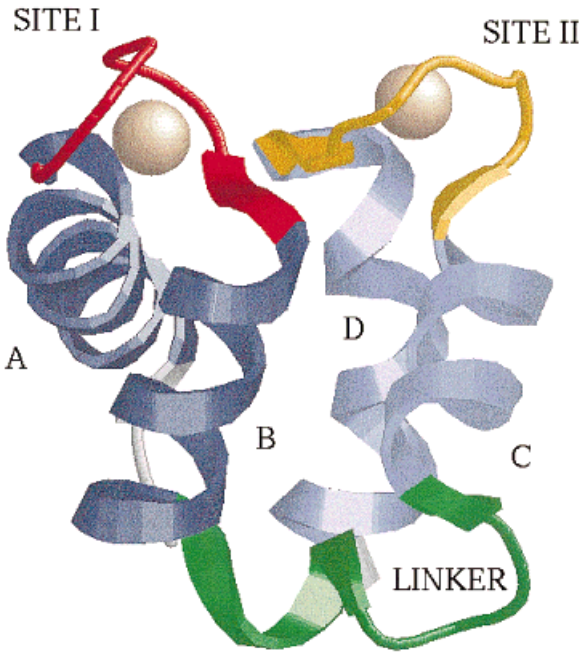

Fig. 1. Schematic representation of calbindin D_{9k} (CAB) with two bound calcium ions. The most important structural elements of CAB are: helix A (3–15), N-terminal site I shown in red (16–24), helix B (25–35), linker shown in green (36–45), helix C (46–53), C-terminal site II shown in yellow (54–62), and helix D (63–73). Two backbone-to-backbone hydrogen bonds, Leu23-O · · · HN-Val61 and Val61-O · · · HN-Leu23, are present between the calcium-binding EF-hand loops.

Although CAB has been the object of previous computational studies,[30–32] the previous studies relied on the structure of the doubly loaded state determined by X-ray crystallography.[18] Åhlstrom et al.[30] and Kördel and Teleman[31] simulated the doubly loaded state of CAB from the crystal structure of Szebenyi and Moffat[18] using the program MUMOD.[33] Mehler et al.[32] used the program CHARMM[34] to simulate all four calcium-loaded states initiated from the X-ray structure of the doubly loaded state.[18]

Recent high-resolution structural data[22,23] makes it possible to extend the current investigation to

other calcium-loaded states. Furthermore, even though the previous computational studies provided insight into the structural and dynamic factors involved in the function of CAB, the simulations suffered from various problems. In particular, the local coordination patterns of the calcium ions as well as some of the secondary structural elements were altered.[30–32] An important difference with the X-ray structure was the involvement of the carboxylate oxygens of Glu60 with the calcium bound in site I, observed in all reported simulations.[30–32] In part, the problems were attributed to the use of an extended-atom representation in which nonpolar atoms are treated as a single particle. Kördel and Teleman[31] showed that the results were in better agreement with experimental data with an all-atom representation, although the fluctuations appeared to be overestimated for all simulations. The current simulations were generated using the protein PARAM22[35] potential function of CHARMM[34] in which all atoms are explicitly included; the nonbonded parameters for Ca^{2+} were determined on the basis of free energy simulations to reproduce the experimental hydration free energy. Additional problems in the previous simulations may have been caused by the limited treatment of electrostatics and solvent.[30–32] Åhlstrom et al.[30] as well as Kördel and Teleman[31] truncated the electrostatic interactions at 10 Å and used periodic boundary conditions with 2,248 explicit water molecules to simulate the solution environment. Mehler et al.[32] used a cutoff of 8 Å, and the surrounding solution was approximated by a 9 Å shell of 1,227 explicit water molecules.

For meaningful quantitative studies of the structural and dynamic factors involved in calcium binding cooperativity, it is important to treat the long-range electrostatics interactions accurately. In particular, because the calcium-to-calcium distance in the doubly loaded state is on the order of 12 Å,[19] a truncation of electrostatic interactions around 8–10 Å implies that the calcium-calcium repulsion (which is on the order of +110 kcal/mol!) is ignored. In addition, the influence of the surrounding bulk solvent, a high dielectric polar medium, is not represented realistically with periodic boundary conditions or with a finite droplet of water molecules.[36] For example, the hydration free energy of Ca^{2+} (−381 kcal/mol in bulk water[37]) is underestimated by more than 30 kcal/mol in a 20 Å radius sphere of water molecules according to the Born model of solvation.[38] In view of the subtle structural rearrangements occurring upon calcium binding[20–23] and the modest free energy of cooperativity involved,[16] it is clear that one must go beyond such approximation to make progress in understanding the function of CAB. Particular attention was given to the treatment of long-range electrostatic interactions in the current investigation. To avoid the truncation and decrease the computational time, the long-range interactions were evaluated with no cutoff using the Extended Electrostatics procedure.[34,39] To avoid periodic boundary conditions, a spherical solvent boundary potential (SSBP) was used to simulate the influence of the infinite surrounding bulk system.[36] The present methodology is more expensive than that used in previous molecular dynamics calculations on CAB,[30–32] but a consistent treatment of electrostatics is essential.

In the Methods section, the construction and assembly of the initial configurations for the apo (A), singly loaded (S_{II}), and doubly loaded (D) states are described, and all the details concerning the simulation procedure and the potential function are given. In the Results and Discussion section, results regarding the structural and dynamic properties are given and compared with experimental data. The paper is concluded with a brief summary of the main results.

METHODS

Microscopic Models and Potential Function

The CAB studied throughout this article is a single-point mutant of the wild-type protein with Pro43 replaced by Gly (P43G). The P43G mutant is often chosen in experimental studies because the Gly42-Pro43 peptide bond of the wild-type protein undergoes a *cis-trans* isomerization,[19] which gives rise to additional and unnecessary difficulties in the analysis of the NMR data.[40] The P43G mutant, which displays only small differences in structure and dynamics from the wild-type protein,[41] is simpler to study experimentally because it possesses a unique conformation. The P43G apo (A) structure[23] and the P43G singly loaded (S_{II}) structure[22] were taken directly from the Brookhaven Protein Data Base. The structures were determined by high-resolution [^{1}H]NMR and refined with restrained molecular dynamics in vacuo. A second trajectory of the A state was generated by removing the calcium ion in the equilibrated S_{II} state. The hydrogen atoms of the three protein structures were constructed using the HBUILD[42] option of CHARMM[34] for a total of 1,195 atoms for the protein. All nonbonded interactions were represented by the Lennard-Jones (LJ) 6–12 potential and coulombic interactions between atomic partial charges. The PARAM22[35] potential function was used for the protein; the TIP3 water model[43] was used to represent all the water molecules included in the systems. The LJ parameters of the calcium ion were optimized to reproduce the experimental free energy of hydration following the approach of Åqvist[44] (see below).

In the case of the doubly loaded (D) state, the structure determined by X-ray crystallography at 1.6 Å resolution[19] rather than the NMR solution structure[20,21] was used because the latter does not provide coordinates for the two bound calcium ions.

Furthermore, the X-ray structure has the advantage of including 57 crystallographic water molecules. Since the X-ray structure has the wild-type sequence, Pro43 was substituted by a glycine to simulate the same system for the three occupancy states. The conformation of the backbone in the vicinity of Gly43 was extracted from the NMR structure[20,21] and substituted in the X-ray structure. To substitute the Pro43 by a Gly, the wild-type X-ray and NMR P43G structure were aligned by minimizing the rms (root-mean-square) distance difference between the C_α excluding amino acid 43 (the final rms difference was 1.91 Å). After the structures were aligned, the coordinates of the C_α, C, O, and the N atoms of Pro43 in the crystallographic structure were replaced by those from Gly43 in the NMR structure. To remove any remaining strain on the structure, this was followed by a short energy minimization of Gly43 and its two neighboring amino acids, keeping the rest of the protein fixed.

The dynamical trajectory of the S_{II} state was generated on the basis of the NMR structure determined with a Cd^{2+} bound in site II.[22] Because the association constants of Ca^{2+} for the site I and II are very similar, singly loaded states cannot be isolated experimentally. For this reason, the experimental structure of the S_{II} state was determined by solution [^{1}H]NMR in the presence of a CD_1^{2+} bound in site II. No large structural difference is expected to arise due to this substitution because Cd^{2+} and Ca^{2+} have very similar radii. Since our purpose is to examine the structure and dynamics of the calcium-loaded states of CAB, the dynamical trajectory of the S_{II} state was nevertheless generated with a Ca^{2+} bound in site II. To model the initial position of the ion (which is not determined by NMR), the atoms of site II of the X-ray structure of the D state were aligned with those of the S_{II} state by minimizing the rms distance difference of between the two structures (the minimum rms difference was 1.17 Å taking into account nonhydrogen atoms only). The calcium-bound water observed in the X-ray structure of the D state was included to replicate the full ion-ligand geometry of site II. A short energy minimization with harmonic restraints applied to the oxygen ligands was performed on all atoms within 5 Å from the calcium to relax the structure of the binding site.

Simulation and Computational Details

The three CAB states were solvated in a sphere of 27 Å radius containing 2,285 water molecules. A spherical solvent boundary potential (SSBP) was used[36] to take the influence of the surrounding solvent into account and obtain statistical properties that are consistent with those of an infinite bulk system. The SSBP was developed to correspond to the statistical mechanical potential of mean force acting on a subsystem from the surrounding bulk water. By construction, it implicitly incorporates the influence of van der Waals interactions and the electrostatic reaction field of the surrounding bulk solvent on the simulated system.[36] The Extended Electrostatics method[34,39] was used to avoid truncating the long-range nonbonded electrostatic interactions. The complete interaction is computed within a normal cutoff (12 Å) and the interaction between the given atom and dipoles and quadrupoles of predefined groups is added for distance lying outside this cutoff. This allows the long-range interactions to be computed in a reasonable time; it requires about 50% longer than the standard nonbonded interactions computed with a cutoff of 12 Å. Since the simulation system contains about 5,000 atoms, an explicit sum over all nonbonded pairs with no truncation at each dynamics time step would be computationally prohibitive. The extended electrostatics method for avoiding the need for truncation is similar in spirit to the fast multipole methods developed more recently.[45]

Langevin dynamics were used to generate statistical ensembles at 300 K, in accord with the temperature of the NMR experiments.[25,26] Langevin and frictional forces were applied to all water oxygen atoms during equilibration. A friction constant corresponding to a velocity relaxation time of 20 ps^{-1} was used. After the equilibration period, Langevin and frictional forces were applied only to the water oxygen lying outside a radius of 22.5 Å from the center of the system. A friction constant of 62.0 ps^{-1} was used.

The length of all bonds involving hydrogen atoms was kept fixed using the SHAKE algorithm.[46] The integration time step was 0.002 ps. The first step in equilibrating the systems consisted in keeping the protein and ions fixed and performing 500 steps of energy minimization followed by 10 ps of dynamics with the protein and ions fixed. For the D state, the 57 crystallographic water molecules were constrained for the energy minimization and the first 5 ps of equilibration. Then the dynamics were run for 25 ps of dynamics with a harmonic restraint of 1.0 kcal/mol/Å^2 applied to the protein, followed by another 25 ps of dynamics with a 0.5 kcal/mol/Å^2 harmonic restraint. Then all restraints were removed and the equilibration protocol was completed by 25 ps of dynamics. A 200 ps trajectory was generated for the A and the S_{II} states. The A trajectory (initiated from the NMR structure of the A state) exhibited the largest fluctuations. For comparison, a second simulation of the A state was generated from the equilibrated S_{II} state (this trajectory is referred to as the A′ trajectory in the remaining of the paper). The calcium ion was removed from the site II and the structure was refined by a cycle of energy minimization (200 steps) and Langevin dynamics (5 ps). The cycle was repeated three times in the presence of a

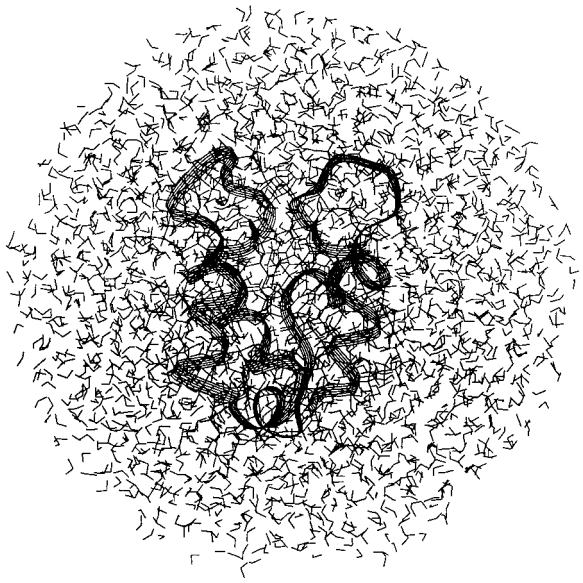

Fig. 2. CAB in the D state solvated by a sphere of 2,285 water molecules after equilibration (the influence of the remaining bulk is taken into account with SSBP).[36]

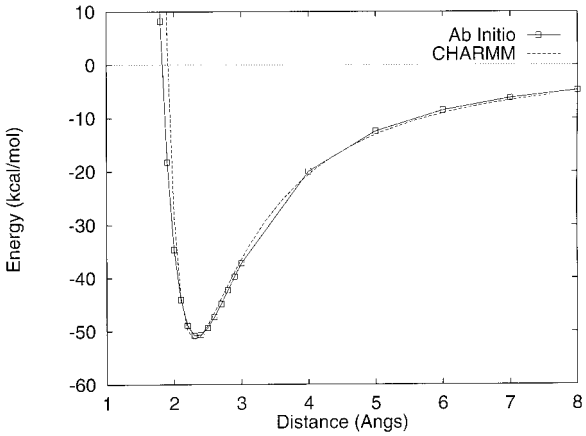

Fig. 3. Interaction between a Ca^{2+} ion and a single water molecule in vacuum. The results from ab initio calculations and from the potential function after adjusting the LJ parameters of the Ca^{2+} to reproduce the solvation free energy in bulk water are shown. The energy was calculated as a function of the ion-oxygen distance along the symmetry axis of the water molecule.

harmonic restraint of 1.0 kcal/mol/Å^2 applied to the protein followed by 75 ps equilibration with no restraints. A trajectory of 200 ps was then generated. Examination of the evolution of the rms differences between the initial and the simulated structures over the simulation period showed that the simulations of the S_{II} and D states had adequate time to relax and equilibrate. The case of the A state is more problematical. For both the A and A′ trajectories, the rms differences between the initial and the simulated structures reached a plateau value of nearly 3.5 Å for the backbone atoms, indicating that the fluctuations are unusually large. For this reason, it is clear that an extensive sampling would be required for a complete quantitative analysis of the A state (i.e., long trajectories initiated from different starting configurations). In the case of the D state, the trajectory was continued for a total of 400 ps to examine the convergence of the results. Unless specifically mentioned, all averages for the D state were performed using the complete 400 ps trajectory. A schematic view of the equilibrated D state with the solvation water sphere is shown in Figure 2.

The LJ parameters of the calcium ion, ϵ and σ, were adjusted to reproduce the experimental free energy of hydration (−381 kcal/mol).[37] The free energy was calculated using a free energy perturbation method[47] with SSBP.[36] The SSBP allowed a rapid parameterization since the LJ parameters were initially adjusted according to the results of free energy simulations performed with a spherical system of only 25 explicit water molecules.[36] After several test runs with 25 explicit water molecules, final adjustments of the LJ parameters were made using spherical systems of 50 and 100 water molecules. The final values for ϵ and σ are −0.12 kcal/mol and 2.435717 Å, respectively. The calculated free energy of charging the ion in the spherical systems of 25, 50, and 100 water molecules was −382, −383, and −385 kcal/mol, respectively. As shown in Figure 3, the resulting empirical potential reproduces the general shape of the interaction between a Ca^{2+} ion and a single water molecule calculated ab initio. The ab initio calculations were performed at the Hartree-Fock level with the gaussian 90 program[48] using the 6-311G** basis sets for the C, H, O, and N atoms, and a contraction of the basis set of Wachters[49] by Gianolo et al.[50] for Ca^{2+}. The basis set superposition error (BSSE) was corrected by the counterpoise method.[51] In the minimum energy conformation, the calcium-water interaction is −50.9 and −50.7 kcal/mol and the ion-oxygen distance is 2.34 and 2.18 Å for the ab initio and potential function, respectively.

RESULTS AND DISCUSSION

Average Structural Properties

Comparison with experimental structures

The average structural properties of the three states calcium-loaded of CAB are first examined. Rms differences, calculated between the initial experimental structure and the average simulated structure, are given in Table I. The average rms differences for the protein backbone (excluding calcium and hydrogen atoms) are 3.30, 1.72, and 1.23 Å, for the A, S_{II}, and D states, respectively. The trajectory of the D and S_{II} states remained close to their initial experimental structures. In contrast, the aver-

TABLE I. Comparison of Average Dynamic Structures With Initial Experimental Structures†

	Structural elements							
	All 1–75	Helix A 3–15	Site I 16–24	Helix B 25–35	Linker 36–45	Helix C 46–53	Site II 54–62	Helix D 63–73
A								
All heavy atoms	3.76	2.02	1.93	1.52	3.33	2.91	4.26	1.54
Backbone	3.31	1.06	1.07	0.48	2.69	1.67	3.65	0.60
C_α	3.30	0.89	0.92	0.48	2.71	1.61	3.65	0.60
A′								
All heavy atoms	3.53	1.52	2.85	1.68	5.12	1.71	3.45	1.80
Backbone	2.78	0.49	1.54	0.46	4.16	0.50	2.55	0.59
C_α	2.79	0.42	1.37	0.47	4.29	0.48	2.48	0.33
S_{II}								
All heavy atoms	2.27	1.35	1.61	0.99	1.38	1.54	1.60	1.36
Backbone	1.75	0.82	1.02	0.38	0.84	0.57	1.06	0.89
C_α	1.72	0.74	1.12	0.36	0.82	0.53	0.81	0.87
D								
All heavy atoms	1.52	1.17	0.95	0.76	1.22	1.04	0.77	1.37
Backbone	1.21	0.59	0.58	0.33	1.05	0.39	0.66	0.76
C_α	1.23	0.56	0.48	0.28	1.11	0.35	0.49	0.77

†Hydrogens are not included in the comparison. The structure A′ was constructed from the S_{II} equilibrated structure by removing the calcium followed by energy minization and molecular dynamics.

age structure of the A state exhibits the largest difference from the experimental structure for all elements of secondary structure (except for helix D and site I). The deviations are the largest for site II and the linker. Nevertheless, a large fraction of the structure of the A state remained close to the initial structure. The rms distance difference, calculated for the backbone of helix A, site I, and helix B together is 1.67 Å, whereas it is 3.56 Å for the backbone of helix C, site II, and helix D together. A visual comparison between the experimental and average simulated structures reveals that the small turn in the middle of the linker as well as helix C is more extended in the simulation than in the initial structure. The orientation of helix C relative to the rest of the structure and site II are modified. Slight deviations in helix A are localized at the N-terminal end.

The deviations of the trajectories appears to be directly related to the magnitude of the dynamical fluctuations of the various calcium-loaded states. The simulation of the D state, which was initiated from a X-ray structure at 1.6 Å resolution, exhibits the smallest deviations. The experimental structure of the S_{II} state is better determined than that of the A state, as indicated by the larger number of NOE distance constraints; the global variation of the ensemble of refined structures for the S_{II} state corresponds to an rms difference of 1.25 Å.[22] Accordingly, the protein remained close to the experimental structure during the dynamic trajectory. The simulation of the A state, which exhibits the largest deviation, was initiated from the structure 1 in an ensemble of 33 structures given in the Protein Data Base file. The global variation of the ensemble of refined structures corresponds to an rms difference of 1.59 Å.[23] However, a closer look at the ensemble of 33 structures reveals that there are large variations in the calcium-binding sites and in helix C. The existence of large fluctuations is reflected in the final resolution of the experimental structure. The authors recognized the limitations of the structural refinement due to insufficient NOE data, saying that: "the relative orientation of helix C with respect to helix D is not well defined."[23]

The regions of the protein having the fewest number of NOE distance constraints in the structure determination are the two termini, the linker region, and the residues at the N-terminal end of each site. The least well determined of all are the backbone atoms of residues 1, 41–43 (linker), 56–57 (site II), and 75,[23] consistent with the observed deviations in the simulation. The difficulties in converging toward a unique structure for the A state based on the experimentally determined NOE distance restraints reflects the important dynamic fluctuations of CAB in the absence of bound calcium. To explore further the properties of the A state and see how they are correlated with initial conditions, a computer experiment was performed. A second simulation of the A state was generated using the equilibrated structure of the singly occupied state S_{II} (hereafter referred to as the A′ trajectory). Results are given in Table I. The A′ trajectory also deviated from the experimentally determined apo structure, although less so than the A trajectory. Interestingly, the dynamic fluctuations of the A′ trajectory are also more important than those of the S_{II} state from which it was initiated (see below). This indicates that the deviations observed

TABLE II. Residues Forming the Calcium-Binding EF-Hands†

Site I (pseudo EF-hands with 14 residues)													
14	15	16	17	18	19	20	21	22	23	24	25	26	27
Ala	Ala	Lys	GLu	GLy	Asp	Pro	Asn	Gln	Leu	Ser	Lys	Glu	Glu
(m)			(m)		(m)			(m)					(s,s)
Site II (standard EF-hand with 12 residues)													
Asp	Lys		Asn	Gly	Asp	Gly		Glu	Val	Ser	Phe	Glu	Glu
54	55		56	57	58	59		60	61	62	63	64	65
(s)			(s)		(s)			(m)					(s,s)

†m, main chain; s, side chain.

in the simulations are due to the intrinsic flexibility of CAB in the absence of bound calcium rather than the choice of initial conditions. In support of that conclusion, further simulations of the A state initiated from different members in the ensemble of 33 structures given in the Protein Data Base file (currently in progress) show a very similar behavior to that of A and A′ (Tenette and Roux, in preparation).

Structure of the binding sites

The ligands forming the calcium-binding site are provided by the loop residues in the EF-hand helix-loop-helix motif (Fig. 1). The sequence of the EF-hands is given in Table II. In the calmodulin superfamily, the standard calcium-binding loop consists of a 12-amino acid sequence.[14] In the binding mode, the calcium ion is coordinated by seven oxygen ligands in a pentagonal bipyramidal configuration. The coordinating ligands in standard EF-hands are five side chain carboxyl oxygens, one backbone carbonyl oxygen, and one water oxygen. The C-terminal calcium binding (site II) spanning residues 54–65 is a standard EF-hand. However, the N-terminal binding site (site I) spans residues 14–27 and has (exceptionally) a 14-amino acid loop region instead of the standard 12-amino acid loop. In this pseudo EF-hand, the calcium ion is coordinated by four backbone carbonyl oxygens, two carboxyl oxygens, and one water oxygen.[19]

During all the simulations the calcium ion(s) remained bound in a stable fashion to the EF-hands. However, small differences between the experimental and simulated average coordination patterns of the calcium ions are observed. The average distances between the ion and its nearest neighbors are given in Tables III and IV. Since there is no information concerning the bound calcium in the S_{II} state, the experimental distances given in Table IV were deduced from the experimental structure by optimizing the position of the calcium, keeping the rest of the protein rigidly fixed (see Methods section). Generally, there is an increased coordination and the ion-ligand distances are slightly shorter than in the X-ray structure (exceptions are Asp19 and Gln22 in the D state). For the D state, one extra water oxygen is added to the seven initial ligands of the experimental structure in site I, whereas the initial coordination pattern remained intact for site II. Interestingly, the carboxylate oxygen of Glu60 is not involved with the calcium bound in site I. This contact, which is not present in the experimental structure,[18–22] was nev-

TABLE III. Ion-Ligand Coordination Structure in State D

	Average ion-ligand distance (Å)	
	Exp†	MD
Site I		
Ala14 O	2.33	2.28 ± 0.08
Glu17 O	2.47	2.36 ± 0.12
Asp19 O	2.25	2.46 ± 0.23
Gln22 O	2.36	2.53 ± 0.22
Glu27 OE1	2.42	2.18 ± 0.06
Glu27 OE2	2.60	2.23 ± 0.08
H_2O O	2.43	2.29 ± 0.56
H_2O O	—	2.54 ± 0.77
Site II		
Asp54 OD1	2.41	2.10 ± 0.05
Asn56 OD1	2.34	2.28 ± 0.09
Asp58 OD1	2.38	2.16 ± 0.06
Glu60 O	2.39	2.28 ± 0.08
Glu65 OE1	2.54	2.20 ± 0.07
Glu65 OE2	2.54	2.30 ± 0.10
H_2O O	2.54	2.26 ± 0.07

†Determined from the 1.6 Å resolution X-ray crystallographic structure.[19]

TABLE IV. Ion-Ligand Coordination Structure in State S_{II}

	Average ion-ligand distance (Å)	
	Exp†	MD (a)
Site II		
Asp54 OD1	2.07	2.31 ± 0.12
Asp54 OD2	—	2.21 ± 0.25
Asn56 OD1	2.15	2.24 ± 0.13
Asp58 OD2	2.11	2.16 ± 0.06
Glu60 O	2.19	2.35 ± 0.11
Glu65 OE1	2.15	2.24 ± 0.11
Glu65 OE2	(3.30)	2.47 ± 0.35
H_2O O	2.53	2.32 ± 2.96

†Constructed on the basis of the NMR structure.

TABLE V. Comparison of Average Dynamic Structures†

	Structural elements							
	All 1–75	Helix A 3–15	Site I 16–24	Helix B 25–35	Linker 36–45	Helix C 46–53	Site II 54–62	Helix D 63–73
A-A′								
All heavy atoms	3.81	1.37	2.01	1.53	4.21	2.04	4.24	1.42
Backbone	3.39	0.86	1.63	0.25	3.49	1.38	2.78	0.67
A-S_{II}								
All heavy atoms	3.34	1.39	1.97	1.37	2.90	1.85	3.23	1.66
Backbone	2.86	0.73	1.55	0.20	2.39	1.34	2.62	0.88
A′-S_{II}								
All heavy atoms	2.57	0.98	1.48	0.83	2.56	0.82	3.33	1.07
Backbone	2.23	0.49	0.93	0.22	1.81	0.37	2.07	0.63
A-D								
All heavy atoms	3.75	1.59	1.93	1.66	3.56	2.47	3.61	2.09
Backbone	3.36	1.15	0.73	0.23	3.11	1.61	2.62	1.37
A′-D								
All heavy atoms	2.64	1.12	2.03	1.21	1.62	1.26	3.24	1.50
Backbone	2.12	0.63	1.64	0.29	1.15	0.41	2.03	1.05
S_{II}-D								
All heavy atoms	2.32	1.37	1.62	0.95	1.98	1.35	1.39	1.43
Backbone	1.83	0.80	1.39	0.24	1.42	0.40	0.80	0.84

†Hydrogens were not included in the comparison.

ertheless observed in all previous simulations of CAB.[30–32] In the case of the state S_{II}, the second carboxyl oxygen of Asp54 added one extra ligand to the calcium for the S_{II} state, giving a total of eight ligands instead of seven. A similar bidendate from the experimental monodendate coordination pattern was observed in the simulation of Mehler et al[32] and Ahlström et al.[30]

It is likely that such deviations from the experimental structure of the binding sites are caused by the neglect of induced polarization in the potential function used for the simulations. It has been shown previously that many-body nonadditive effects due to ion-induced polarization effects can be significant in the case of small ions such as Li^+ and Na^+.[52] A computational study of sodium in the binding site of the gramicidin channel based on a limited treatments of induced polarization showed that the structure of the coordination shell and the number of ion ligands can be affected by nonadditive effects.[53] According to this analysis, the slightly underestimated ion-ligand distances in Tables III and IV are consistent with the lack of nonadditive polarization.[52] In the current calculations, the electrostatic interactions were approximated with fixed atomic partial charges to retain the standard potential function used in most biomolecular simulations. To make sure that the nonbonded interactions were well balanced, the LJ parameters of the calcium ion were adjusted to reproduce the experimental hydration free energy of hydration. As a result, the structural deviations are small and localized to the nearest neighbors of the calcium ion in the binding sites. Because the overall fold of the calcium-loaded states is in excellent agreement with experimental data, we believe that further analysis of the simulations is meaningful despite the limitations of the current model.

Comparison of the three calcium-loaded states

In Table V the various calcium-loaded states are compared by calculating the rms difference. The S_{II} and D states appear to be structurally similar with rms differences of only 1.83 Å between main chain atoms (2.23 Å including all heavy atoms). The structure of the A state shows the largest difference with the two other states, although it appears to be slightly closer to the S_{II} state than to the D state. Helices A, B, and D, as well as site I, appear to be little affected by the binding of calcium. The rms between the D and S_{II} state is 1.62 Å for site I (all heavy atoms); it is 1.97 and 1.93 Å between state A and S_{II}, and A and D, respectively. In contrast, the linker, helix C, and site II are affected to a different extent. There is an alteration of the linker and helix C by the successive binding of a first and a second ion. Site II appears to undergo the largest structural changes upon binding of the first ion. For site II the rms between the D and S_{II} state is 1.39 Å (all heavy atoms); the rms between the A and S_{II} state, and between the A and D state is 3.23 and 3.63 Å, respectively. The average structure resulting from the A′ trajectory is closer to both the S_{II} and D states. However, it is possible that the A′ trajectory, initiated from the experimental structure of the S_{II} state, did not have enough time to forget its starting point completely. The large fluctuations of the protein in

the absence of calcium makes further comparison in terms of average structures difficult.

An alternative view of the structural changes upon calcium binding is provided by examining the compactness of the protein. To characterize the variations in the compactness of the calcium loaded states, average intramolecular distance maps were calculated. Plots of backbone atoms (excluding H_α) separated on average by less than 5 Å are shown in Figure 4. The dashed lines outline the residues forming the EF-hand binding sites. The results for both the A and A′ (not shown) trajectories are similar. The contact plots show that the protein becomes progressively more compact going from the A, to the S_{II}, to the D state and that the S_{II} and D states have similar structures that are both different from that of the A state. The A state exhibits internal backbone-backbone contacts in site I but none in site II. The S_{II} state has a similar number of contacts in site I, additional internal contacts in site II, and a large number of contacts between site I and site II. Compared with the S_{II} structure, the D state has several new internal contacts in site I but the same contacts in site II. There are 14 and 20 backbone-backbone contacts between site I and II according to the A and A′ trajectories, respectively. In contrast, there are 52 such contacts in the S_{II} state and 41 in the D state.

Protein hydration

Variations in the compactness of the protein structure are expected to be correlated with corresponding variations in the solvent exposure. As the protein interacts strongly with the bound calcium ion(s), some structural elements become increasingly shielded from the solvent. Since water molecules are included explicitly in the present simulations, a natural approach to characterize solvent exposure is to examine the protein-solvent radial distribution functions for all backbone and side chain atoms. To reduce the amount of information, an effective residue-based hydration number was calculated by integrating the radial distribution functions to a distance of 4 Å and by performing an average for all atoms within a residue (backbone or side chain). The results are shown in Figure 5. Qualitatively, the solvation profile for both backbone and side chains is similar for all three states, reflecting the fact that there are no large conformational change upon calcium binding. The hydration of the side chains varies progressively with calcium binding. The backbone atoms of the apo state are slightly more exposed to water than those of the S_{II} and the D states. The binding of a first ion in site II is correlated with a dehydration of the backbone at site I (residues 21–26), and at the linker (residues 36–41). The side chains of site II (residues 54–59) are more affected by the presence of a calcium than those of site I. This is consistent with the fact that the ion is bound to five side chain oxygens in site II, whereas only two side chain oxygens bind the ion in site I. The results from the A′ trajectory (not shown) are similar. The present analysis is made possible by the presence of explicit solvent molecules. For instance, no significant variations in the solvent-exposed surface area of the backbone and side chains are observed upon calcium binding using standard algorithms.[54]

In Figure 6, representative configurations of the calcium-binding sites taken from the end of the trajectories of the D, S_{II}, and A states are shown to illustrate the progressive structural changes taking place as calcium ions are replaced by water molecules in sites I and II. For the sake of clarity, only the water molecules closer than 3 Å from the EF-hands oxygen ligands are shown. In the D state, the ion-ligand complex is very tight, and only one or two nearby water molecules are present. In the S_{II} state, the calcium ion in site I is replaced by two water molecules, simultaneously forming hydrogen bonds with the side chain of Glu27 and the backbone carbonyl oxygens of Ala14 and Gln22. Nevertheless, it is observed that the overall conformation of site I is remarkably similar to that of the D state. The backbone of Glu17 exhibits the largest structural deviation from the D state, whereas the five ligands provided by Ala14, Asp19, Gln22, and Glu27 retain the same configuration. In going from the S_{II} to the A state, the conformation of site I is undergoing further modifications. Glu17 is now moved away relative to its position in the S_{II} and D states. Nevertheless, the backbone carbonyl of Asp19 and Gln22 remains in a configuration reminiscent of the D state, whereas Glu27 and Ala14 are only displaced slightly (there is a local isomerization of the side chain in the case of Glu27). The largest modifications in site II occur for the A state. Residues Asp54 and Asn56 completely leave the binding site region to be solvated by water molecules. Residues Asp58, Glu60, and Glu65 remain in a configuration very similar to those of the D and S_{II} states. Despite the difference in sequence, the three most stable residues in both binding sites have a clear relationship according to the EF-hand structure (Table II): Asp19 (main chain), Gln22 (main chain), and Glu27 (side chain) in site I and the corresponding residues Asp58 (side chain), Glu60 (main chain), and Glu65 (side chain) in site II. Similarly, the residues with the largest structural change are Glu17 in site I and, correspondingly, Asn56 in site II. Those residues are connected to helix A (site I) and helix C (site II). The most stable structural elements are connected to helices B and D, which belong to the central core of the protein. The two backbone-backbone hydrogen bonds, between Val61 and Leu23, are present in the three states. The hydration pattern observed for the A state is remarkably similar for the two calcium-

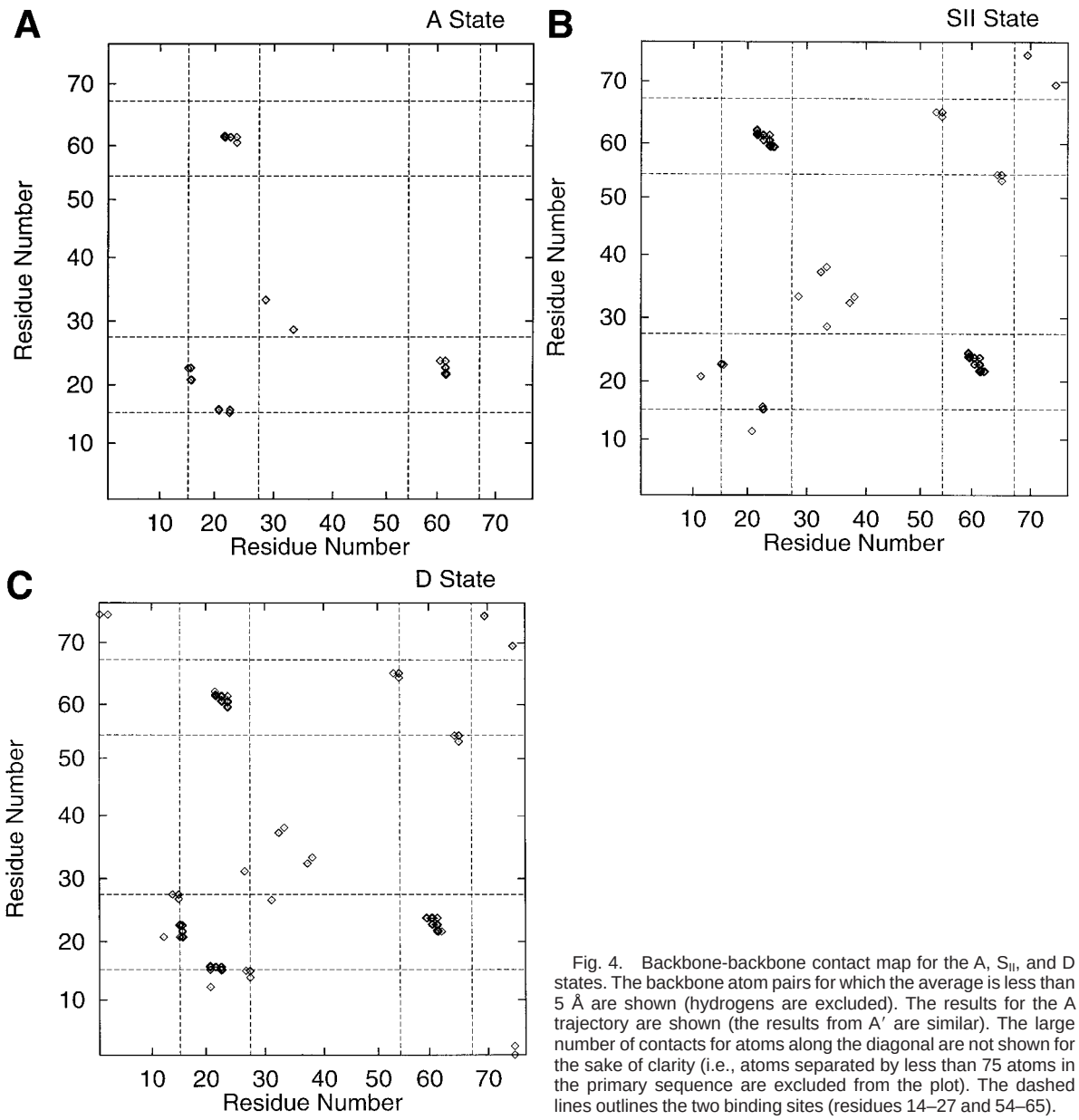

Fig. 4. Backbone-backbone contact map for the A, S_{II}, and D states. The backbone atom pairs for which the average is less than 5 Å are shown (hydrogens are excluded). The results for the A trajectory are shown (the results from A′ are similar). The large number of contacts for atoms along the diagonal are not shown for the sake of clarity (i.e., atoms separated by less than 75 atoms in the primary sequence are excluded from the plot). The dashed lines outlines the two binding sites (residues 14–27 and 54–65).

binding sites. In site I, two water molecules are forming hydrogen bonds with the backbone carbonyl groups of Asp19 and Gln22; the side chain of Glu27 is hydrated by four water molecules. Similarly, three water molecules form hydrogen bonds with the carbonyl groups of Glu60 and the side chains of Asp58 and Glu65 in site II. Both Glu17 and Asn56 exhibit large displacement relative to their configuration in the D state, making contact with solvent molecules.

Fluctuations and Dynamical Properties

Crystallographic B-factors

The trajectories provide a wealth of information concerning the dynamics and flexibility of CAB in the different calcium-loaded states. To assess the validity of the simulations, it is important to compare the calculated protein fluctuations with available experimental data. Assuming that there is no static disorder in the crystal, the crystallographic Debye-Waller *B*-factors provide information about the rms atomic fluctuations of the protein[55]:

$$\langle \Delta r_i^2 \rangle = \left(\frac{3}{8\pi^2} \right) B_i. \qquad (1)$$

In Figure 7, the rms fluctuations calculated from the simulation of the D state are compared with the

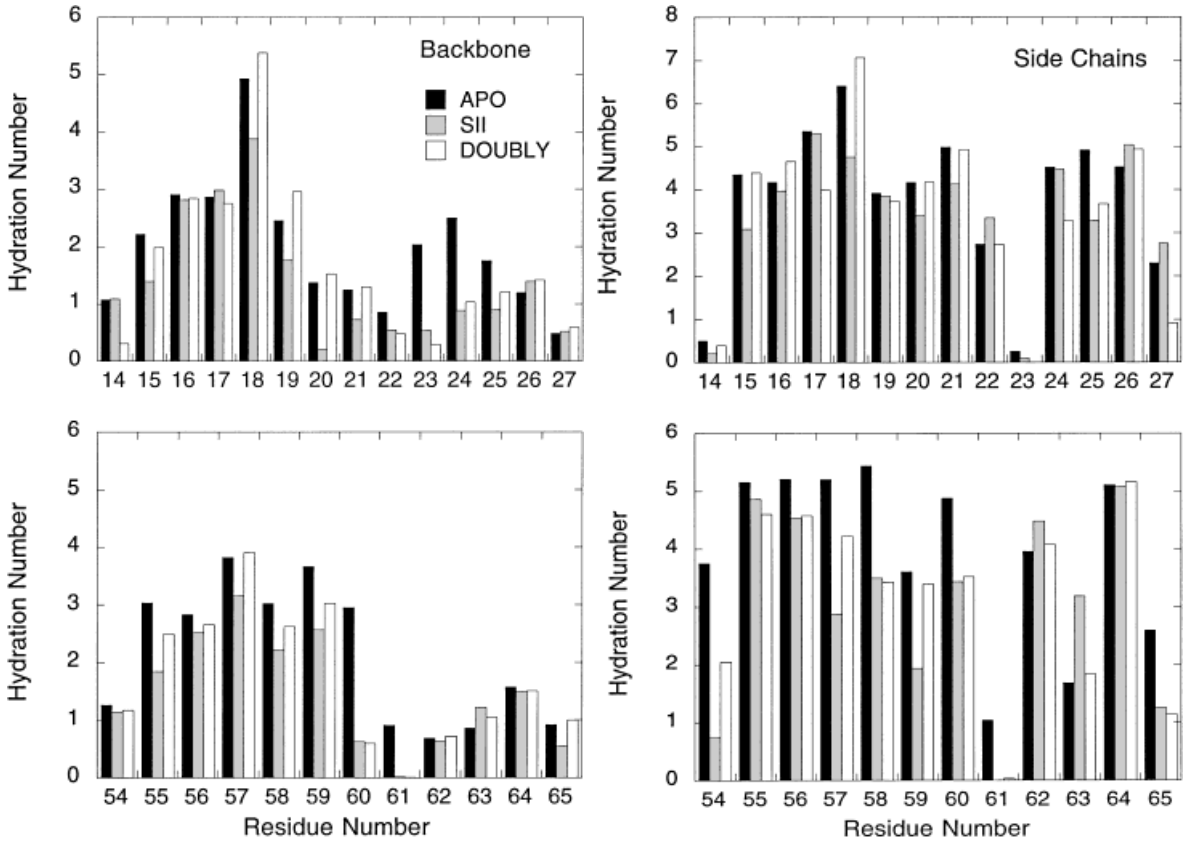

Fig. 5. Average solvent exposure for the A (black), S_{II} (gray), and D (white) states. The results for the A trajectory are shown (the results from A′ are similar). The number of water molecules within a distance of 4 Å from each amino acid is shown for backbone (left) and side chains atoms (right). Protein hydrogens were included in the average.

atomic fluctuations extracted from the crystallographic *B*-factors.[18] Although the deviations are slightly larger in the terminal regions, the lower boundary of the envelope of fluctuations, which corresponds to the backbone atoms, is essentially the same in experiment and simulation. Generally, the side chains are slightly more flexible in the simulation. This may be expected because the simulated environment corresponds to a bulk solution.

The crystallographic *B*-factors were determined for the native CAB, and the trajectory was generated for the P43G mutant, which is commonly studied experimentally.[19,22,23,40,41] The atomic fluctuations are expected to be larger with a glycine in this position since this amino acid allows more backbone flexibility than a proline. Thus, the smaller fluctuations in the X-ray structure near residue 43 are probably due to the difference in amino acid sequence. The fluctuations of a few residues of site I (e.g., Asp18, Pro19, and Asn20) are overestimated, whereas those of the linker region (Gln33 to Lys41) are slightly underestimated. The side chains with the largest fluctuations are generally the lysines (7, 29, and 71), which are more flexible than the average. In addition, Glu11, Glu26, and Gln33 in site I, as well as Glu51 and Glu64 in site II exhibit large fluctuations both in the X-ray data and in the MD trajectory. For those residues, there is an excellent quantitative agreement between the simulation and the X-ray (the rms fluctuations are on the order of 1.1–1.2 Å). Two residues with large fluctuations, Glu26 and Glu64, have corresponding positions in the EF-hands (Table II). In contrast, the side chains of Glu27 and Glu65, which provide two ion ligands in a bidendate configuration, only have rms fluctuations of 0.60 and 0.70 Å, respectively. In both the X-ray data and the trajectory, the two regions with the smallest rms fluctuations are the backbone atoms of Leu23 and Val61 (the rms are on the order of 0.5 to 0.6 Å). Interestingly, these two residues form a short β-strand with two backbone-backbone hydrogen bonds bridging the two calcium-binding EF-hands. The backbones of the residues in site I exhibit smaller fluctuations than those of site II. This is consistent with the fact that four backbone carbonyl oxygens (Ala14, Glu17,

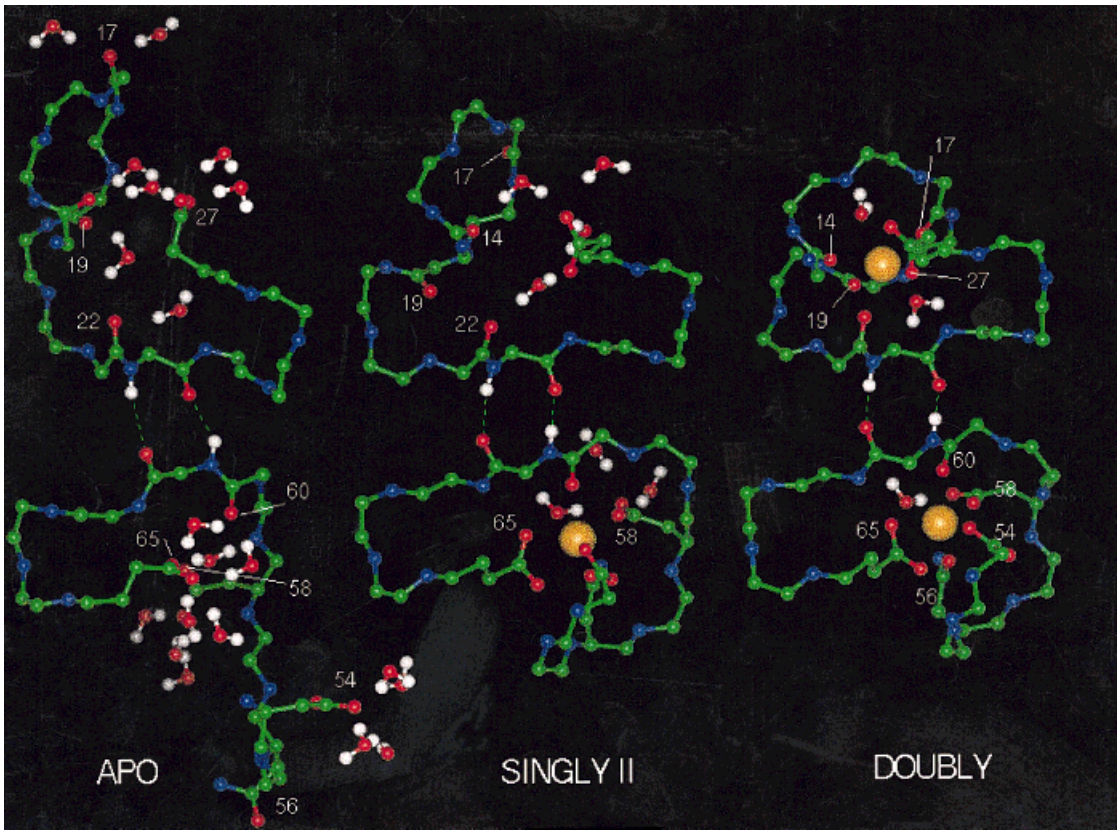

Fig. 6. Molecular graphics representation of the site I (top) and II (bottom) extracted from the A′ (left), S_{II} (middle), and D (right) simulations at the end of the trajectory (200 ps). The view is looking outward from the protein center. The backbone-backbone hydrogen bonds between Leu23 and Val61 are present in the three calcium-loaded states. The residues Asp19 (main chain), Gln22 (main chain), and Glu27 (side chain) in site I, and the corresponding residues Asp58 (side chain), Glu60 (main chain), and Glu65 (side chain) in site II form the most stable structural element in the two binding sites.

Asp19, and Gln22) are involved in calcium binding in site I.

Generally, the good agreement between the calculated rms fluctuations and the values extracted from the crystallographic *B*-factors indicates that the overall flexibility of the protein in the D state is described realistically by the simulation. A similar comparison is not possible in the case of the A and S_{II} calcium-loaded states because the rms atomic fluctuations are not available since those structures were determined by NMR.[22,23]

NMR backbone order parameters

Determination of backbone order parameters through NMR relaxation measurements represents a powerful approach to characterize the dynamic fluctuations of a macromolecule in solution.[56–58] Briefly, the NMR order parameter S_{ij}^2 for a pair of atoms *i* and *j* corresponds to the plateau value of the dipole-dipole correlation function in the molecular frame.[58–60] It is expressed as a time-average:

$$S_{ij}^2 = \frac{4\pi}{5}\sum_{m=-2}^{2}\left\langle\frac{1}{r_{ij}^6}\right\rangle^{-1}\left|\left\langle\frac{Y_{2m}(\theta_{ij}^{(\mathrm{mol})}(t),\,\phi_{ij}^{(\mathrm{mol})}(t))}{r_{ij}^3(t)}\right\rangle\right|^2, \quad (2)$$

where Y_{2m} is a spherical harmonic function and $(r_{ij},\ \theta_{ij}^{(\mathrm{mol})},\ \phi_{ij}^{(\mathrm{mol})})$ represent the $(\mathbf{r}_i^{(\mathrm{mol})} - \mathbf{r}_j^{(\mathrm{mol})})$ atom-atom vector expressed in spherical coordinates in the molecule-fixed reference frame. The internuclei distance $r_{ij}(t)$ may be omited from the expression if, as in the present simulations, the N-H bond length is constrained.

The backbone N-H and C_α-H_α bond vectors were calculated for the A, S_{II}, and D calcium-bound states using Eq. (2). To perform the averaging in the molecule-fixed frame, each snapshot of the trajectory was reoriented by minimizing the rms difference with respect to a reference structure to remove the global rotational motion. The experimental values were obtained, via the model-free of Lipari and

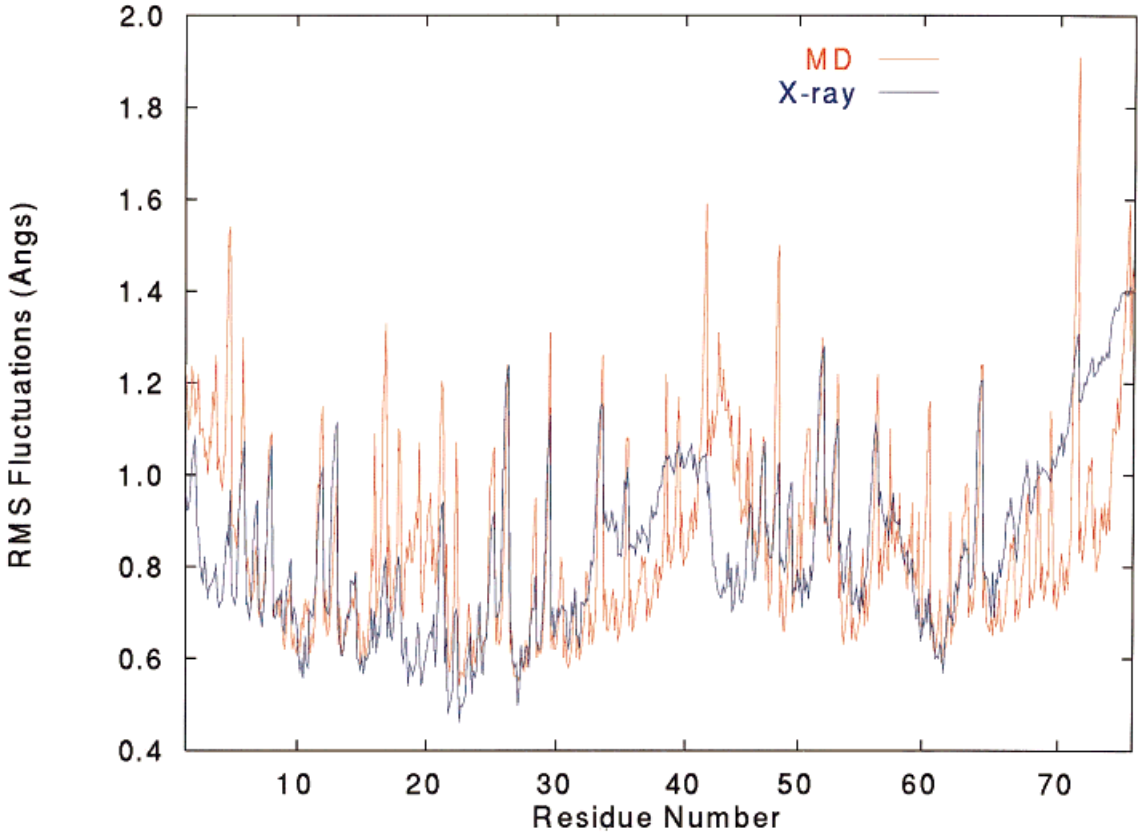

Fig. 7. RMS fluctuations of the doubly loaded state D compared with values extracted from X-ray crystallography *B*-factors[18] (hydrogen atoms are not included).

Szabo,[61] from an analysis of the ^{15}N relaxation rate constants $1/T_1$, $1/T_2$, and NOE.[25,26]

The calculated and experimental values of the backbone N-H bond order parameters are shown in Figure 8A and B. Averages over the secondary structure elements are compared in Table VI. The calculated C_α-H_α order parameters are shown in Figure 8C. The corresponding data for the C_α-H_α bond order are not yet available (W.J. Chazin, personal communication). The most important trend is reproduced: the A state is the most flexible, whereas the S_{II} and the D states are similar.[25,26] Furthermore, the presence of a single calcium bound to site II is correlated with a loss of structural flexibility in site I, as observed in the experiment. The flexibility of the linker region is highest for the D state, as observed in the experiments. A similar trend is observed for the C_α-H_α backbone order parameters upon binding of calcium, although the variations are less important than for the N-H order parameters. The calculated N-H order parameters have smaller values than the C_α-H_α order parameters. In the helices, the calculated N-H order parameters are on the order of 0.89, whereas the corresponding C_α-H_α order parameters are on the order of 0.95. This is expected since N-H order parameters are dominated by the magnitude of the local librations of the peptide plane (i.e., concerted fluctuations of the neighboring ϕ_i and ψ_{i-1} torsion angles are responsible for the order parameters for the ith residue).[62] In contrast, such concerted reorientational motions cannot freely occur for the C_α. From this point of view, the C_α-H_α order parameters can provide an alternative perspective on the global flexibility of the backbone.

According to Eq. (2), a value of S_{ij}^2 close to 1 is indicative of structural rigidity, whereas a value close to 0 is indicative of a structural flexibility with large amplitude fluctuations. In principle, the presence of dynamic fluctuations necessarily decreases the value of the order parameters. However, when order parameters are calculated from a finite trajectory, the results depend on the extent of the conformational sampling. To address issues of convergence, the trajectory of the D state was extended to 400 ps. No differences was observed for the order parameters calculated from the 200 ps and 400 ps trajectories. Further analysis showed that the backbone sites fluctuated over a single configuration with no

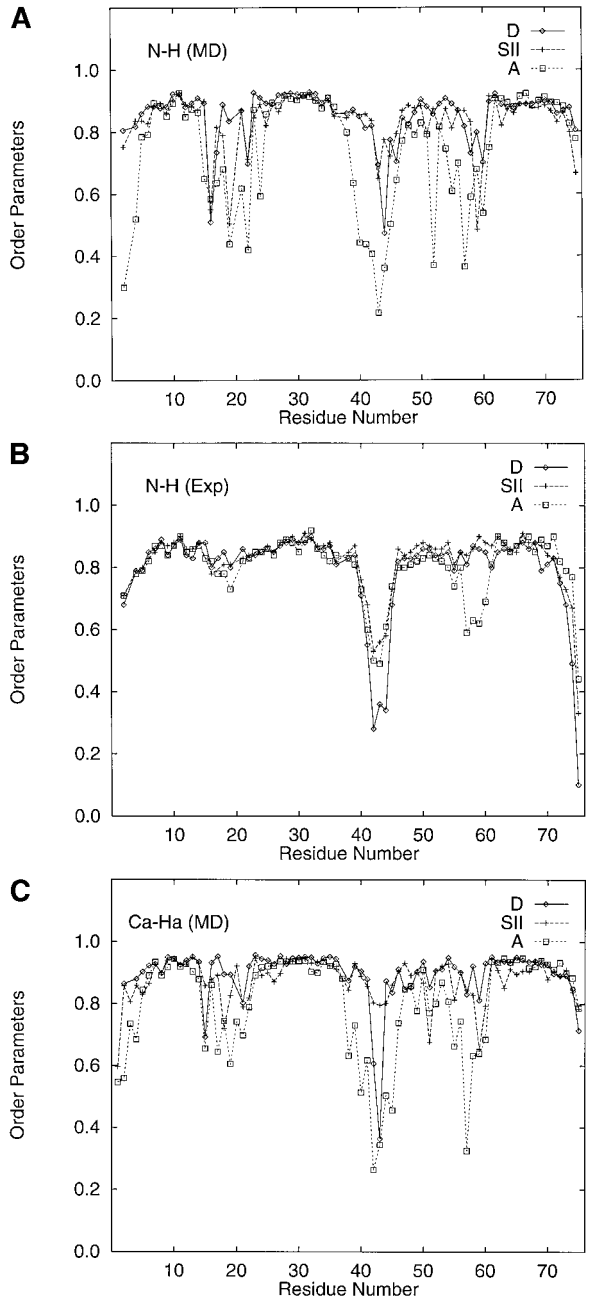

Fig. 8. Generalized backbone order parameters S^2 for the A, S_{II}, and D states. The results for the A trajectory are shown (the results from A′ are similar). **A:** Backbone N-H order parameters calculated from the trajectories. **B:** Backbone N-H order parameters from experiment.[25] **C:** Backbone C_α-H_α order parameters calculated from the trajectories.

abrupt jump-like transitions. This indicates that the conformational sampling of the D state is sufficient. Since the S_{II} state is structurally and dynamically similar to the D state, it is expected that the sampling is adequate for this case as well. In addition, both the D and S_{II} trajectories remained close to the experimental structure (the backbone rms are 1.21 and 1.75 Å, respectively). A quantitative characterization of the A state is more difficult because the protein undergoes large dynamic fluctuations. As seen from Table VI, the order parameters calculated from the A and A′ trajectories are similar. Nevertheless, the results from both trajectories indicate that there are large dynamic fluctuations in the absence of calcium.

The N-H order parameters result from a combination of molecular motions that cannot be directly interpreted in terms of backbone dihedral fluctuations. Nevertheless, the variation in protein flexibility exhibited by the NMR order parameters is clearly reflected in the average rms fluctuations of backbone ϕ and ψ dihedral angles shown in Figure 9. On average the fluctuations are on the order of 10–15 degrees, except in the calcium-binding sites and in the linker region, where the fluctuations are on the order of 20–30 degrees. There is a noticeable change in the protein flexibility upon calcium binding. The S_{II} state shows smaller fluctuations than the A state in the linker, in site II, as well as in site I. Helix C (located between the linker and site II) is more flexible than the other helices. This is more so for the A state. Similar trends were observed in the fluctuations of the cartesian coordinates (data not shown).

To characterize further the dynamic motions of the backbone, we used an empirical expression relating the dihedral fluctuations $\langle \delta\phi_i^2 \rangle$ and $\langle \delta\phi_i^2 \rangle$ to the order parameters of the two neighboring amide planes $\langle S_i^2 \rangle$ and $\langle S_{i+1}^2 \rangle$

$$\langle \delta\phi_i \rangle = [1 - C_1\langle S_i^2 \rangle - C_2\langle S_{i+1}^2 \rangle] \times 60 \text{ degrees}, \quad (3)$$

and

$$\langle \delta\psi_i \rangle = [1 - C_3\langle S_i^2 \rangle - C_4\langle S_{i+1}^2 \rangle] \times 60 \text{ degrees}. \quad (4)$$

The coefficients are normalized ($C_1 + C_2 = 1$ and $C_3 + C_4 = 1$) so that order parameters equal to 1.0 correspond to the absence of backbone fluctuations by construction ($\langle \delta\phi_i \rangle =$ and $\langle \delta\psi_i \rangle = 0$). The coefficients C_i were obtained by least-square fitting. A total of 130 entries were used in the least-square fitting (including the calculated order parameters $\langle S_i^2 \rangle$ and the fluctuations $\delta\phi_i$ and $\delta\psi_i$). Only the backbone sites with order parameters larger than 0.5 taken from the 400 ps simulation of the D state, which are in best agreement with the experimental data, were used. The resulting coefficients C_i are 0.62, 0.38, −0.22, and 1.22, for $i = 1$ to 4, respectively. On average, the values predicted by the empirical relations Eqs. (3) and (4) deviate by 4 degrees from the values extracted directly from the trajectory. Because of the exclusion of the lowest values in the least-square fitting procedure, it is

TABLE VI. Average Backbone Order Parameters

	Structural elements					
	Helix A 4–14	Site I 16, 18–22	Helix B 25–35	Helix C 46–54	Site II 55–62	Helix D 63–73
A						
Exp	0.85 ± 0.01	0.80 ± 0.02	0.87 ± 0.01	0.82 ± 0.01	0.72 ± 0.04	0.86 ± 0.01
MD	0.83 ± 0.10	0.55 ± 0.10	0.90 ± 0.02	0.73 ± 0.14	0.64 ± 0.15	0.90 ± 0.01
A′						
MD	0.90 ± 0.02	0.63 ± 0.15	0.91 ± 0.01	0.86 ± 0.03	0.66 ± 0.10	0.87 ± 0.03
S_{II}						
Exp	0.85 ± 0.01	0.82 ± 0.01	0.880 ± 0.004	0.863 ± 0.005	0.86 ± 0.01	0.84 ± 0.02
MD	0.87 ± 0.03	0.74 ± 0.14	0.91 ± 0.03	0.73 ± 0.04	0.85 ± 0.13	0.86 ± 0.02
D						
Exp	0.84 ± 0.01	0.82 ± 0.02	0.862 ± 0.004	0.838 ± 0.005	0.83 ± 0.01	0.82 ± 0.02
MD	0.87 ± 0.04	0.75 ± 0.13	0.91 ± 0.01	0.86 ± 0.07	0.82 ± 0.10	0.88 ± 0.01

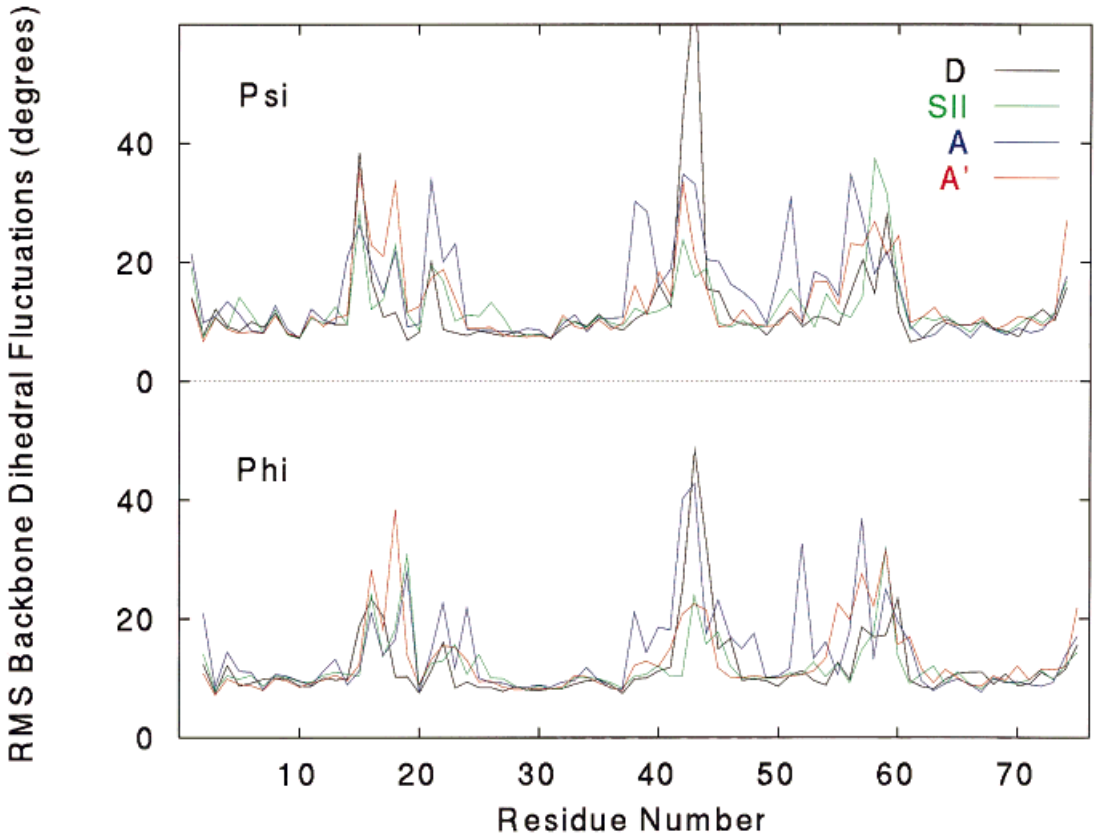

Fig. 9. RMS backbone dihedral angle fluctuations ψ (top) and ϕ (bottom) for the A, S_{II}, and D states (the results for the A and A′ trajectories are shown for comparison).

likely that the empirical relation is accurate only for $\langle S_i^2 \rangle$ larger than some lower bound. The present analysis differs from the mechanical models that have been previously proposed to describe the motions of the backbone motions and its influence on the N-H order parameters.[27,63,64]

The empirical relation represents a simple expression of the statistical correlation between the motion of a peptide linkage and the resulting N-H reorientation. Although the coefficients were obtained by relating the calculated order parameters and calculated backbone dihedral fluctuations extracted from a trajectory, the empirical relation may be used with experimental order parameters to estimate the magnitude of the dihedral fluctuations. The empirical relation suggests that values of $\langle S_i^2 \rangle$ around 0.8

correspond to dihedral fluctuations on the order of 12 degrees, whereas values around 0.7 correspond to dihedral fluctuations on the order of 18 degrees. This analysis shows that the N-H backbone order parameters are sensitive to small variations in the magnitude of backbone fluctuations.

Generally, the value of the order parameters is close to 1 for the residues located in the helices. In contrast, the value of the order parameters is smaller for the residues located in the calcium-binding sites and the linker, indicating that those regions are flexible. For some residues, the calculations shows important deviations from the experimental data. For example, the calculated N-H order parameter of Lys16 for the D state is too small compared with the experimental value, indicating that the fluctuations of the backbone in this region are overestimated in the simulations. It is likely that the underestimated calculated order parameters relative to the experimental data in the EF-hands imply that the local protein flexibility is overestimated by the force field in the regions lacking secondary structure. This observation is consistent with previous comparisons between experimental order parameters and values calculated from simulations.[31,62,65–69] One study of hen lysozyme[62] found that the order parameters from the simulations had higher variability along the peptide backbone than in the experiments (e.g., a number of residues had low-order parameters compared with their near neighbors in the primary sequence). It was concluded that the small-order parameter value arose mostly from peptide librations and concerted backbone dihedral transitions. Because they do not possess as many stabilizing backbone hydrogen bonds, regions with little secondary structure provide a stringent test of the backbone torsion potential. For example, order parameters calculated from a molecular dynamics trajectory generated with the extended atom PARAM19 force field of CHARMM were in excellent agreement with experimental data in the case of *Escherichia coli* ribonuclease H_1, a protein rich in hydrogen bonded secondary structure.[69]

Coupling Between the EF-Hands

According to the NMR data, the dynamic fluctuations of the protein are significantly reduced after the binding of a first calcium ion.[25,26] This important trend is also observed in the current molecular dynamics trajectories (see above). As first noted by Akke et al.,[27] such a reduction in fluctuations is consistent with an important entropic contribution to the cooperativity of calcium binding. From a structural and dynamical point of view, the reduction in protein fluctuations indicates that the flexibility of one EF-hand binding loop is affected by the presence of calcium in the other EF-hand binding loop. Since the pair of EF-hands forms the functional unit enabling the cooperative calcium binding, it is important to examine possible molecular mechanisms that can give rise to the observed coupling between the two EF-hands.

Variations in the packing of nonpolar side chains upon calcium binding are observed in the simulations. Such changes in the packing are best illustrated by the contact maps shown in Figure 4. According to the average contact maps, the structural environment of some nonpolar residues exhibits large variations upon calcium binding. In particular, Val61 is involved in the largest number of contacts between site I and site II (Fig. 4). To examine the role played by the nonpolar contacts on cooperativity, the distributions of the van der Waals (vdW) interaction energy between the side chain of Val61 and the rest of the protein was calculated in the three calcium-loaded states. The distribution functions of the vdW interaction energy are shown in Figure 10. The distributions have a half-width of approximately 3 kcal/mol and overlap considerably. Nevertheless, the distributions show that the energy is increasingly favorable for the calcium-loaded states with higher occupancy. The average interaction energy is −7.34, −9.36, and −9.72 kcal/mol for the A, S_{II}, and D states, respectively. The average for the A′ trajectory is −7.68 kcal/mol and does not differ markedly from the average for the A trajectory. The variation in the interaction energy is consistent with the fact that the structure of CAB becomes more compact upon calcium binding. Recent site-directed mutagenesis data showed that substitution of Val61 by an alanine reduces the cooperativity (S. Linse, personal communication). In view of this result, the variation in the vdW energy distributions shown in Figure 10 is suggestive. The present analysis, based on molecular dynamics trajectories, includes the spontaneous fluctuations occurring at room temperature for the three states. Because the fluctuations in interaction energies are considerable, an analysis based on a single static configuration for each state would not be meaningful. In particular, the van der Waals interaction energies evaluated from the initial experimental structures (−9.89, −9.55, and −10.57 kcal/mol, for the A, S_{II}, and D states, respectively) are not in the same order as the corresponding averages from the simulations.

A different mechanism giving rise to a coupling between the EF-hands is provided by hydrogen bonding. Leu23 and Val61 form a short β-strand introducing a direct interaction between the residues of the binding loops (Figs. 1, 6). Analysis shows that the two hydrogen bonds, Leu23-O · · · HN-Val61 and Val61-O · · · HN-Leu23, may be affected by calcium binding. The radial distributions of the hydrogen bonding distance calculated from the simulations are shown in Figure 11. The distribution functions from both the S_{II} and the D states are

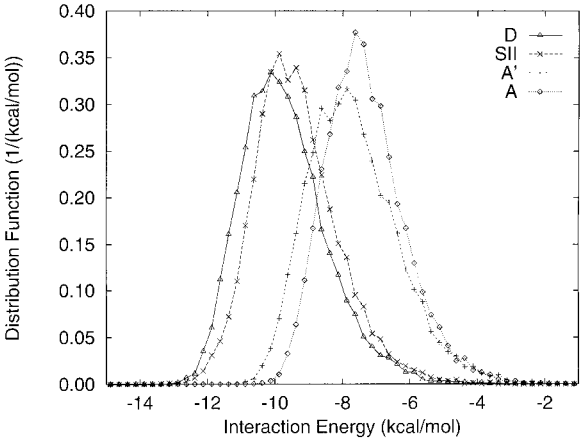

Fig. 10. Distribution of the van der Waals potential interaction energy between the side chain of Val61 and the rest of the protein for the A′, S_{II}, and D states.

considerably sharper than those from the A state. In both A and A′ the fluctuations are important, giving rise to broad radial distribution functions. The two hydrogen bonds are present in both the S_{II} and the D states. During the A trajectory, a water molecule inserted between the Leu23 O and the Val61 HN, forming a bridge between the two residues. As a consequence, the Leu23-O ··· HN-Val61 bond is broken and the Val61-O ··· HN-Leu23 bond is weakened. Although there are important fluctuations, both hydrogen bonds remain stable in the A′ trajectory, which was initiated from the singly loaded structure. Further trajectories of the A state currently in progress show a similar sensitivity of the Leu23-Val61 hydrogen bonds (Tenette and Roux, in preparation). An extensive sampling of the A state (a folded protein with unusually large dynamic fluctuations) will be required for a full quantitative analysis of the stability of the Leu23-Val61 hydrogen bonds. Nevertheless, the observed sensitivity of these hydrogen bonds to the presence of calcium suggests that this could be an important coupling mechanism between the EF-hands.

SUMMARY AND CONCLUSION

Molecular dynamics simulation were performed for the apo, the singly, and the doubly loaded states of calbindin D_{9k}. The structures determined experimentally by X-ray[17,18] and by NMR[20–23] were used to initiate the simulations. The present trajectories were generated with no truncation of the electrostatic interactions and a solvent boundary potential to mimic the reaction field from the bulk and avoid periodic boundary conditions. Such a consistent treatment of electrostatics cannot be avoided for a meaningful investigation of calcium-binding proteins.

Throughout the trajectories, the S_{II} and the D states remained very close to their respective initial

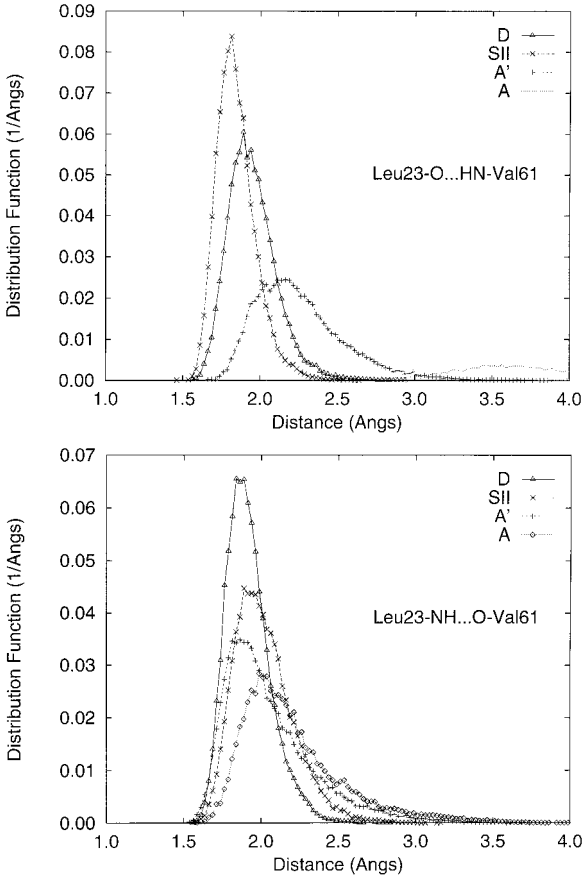

Fig. 11. Radial distribution functions of hydrogen bond lengths for the A, A′, S_{II}, and D states. Top, hydrogen bond between the backbone carbonyl oxygen of Leu23 and the amide hydrogen of Val61. Bottom, hydrogen bond between the amide hydrogen of Leu23 and backbone carbonyl oxygen of Val61.

experimental structures, and analysis indicates that the average results for these two states are converged. In contrast, the A state exhibited larger rms differences from the initial experimental structure. Most of the deviations in the A state were localized in site II, helix C, and the linker region. For comparison, a second trajectory of the A state was generated by removing the calcium ion from the equilibrated structure of the S_{II}. The properties of the second trajectory were similar to those of the first trajectory, although the deviation from the experimentally determined apo structure were somewhat less important. Since both trajectories of the A state behave in a similar fashion, we conclude that the deviations are not caused by the initial conditions, but by the large fluctuations due to the absence of bound calcium. Further work is currently in progress to explore the large conformational space accessible to the A state using different initial conditions based on the NMR data (Tenette and Roux, in preparation). Preliminary results show that similar dynamic fluctuations are observed in these trajectories of the A state.

Calculated dynamic properties are in good accord with experimental data. The experimentally observed trend in the NMR order parameters is reproduced: the A state is the most flexible, and the S_{II} and the D states are similar.[25,26] The binding of calcium seems to affect dynamics by inducing a loss of flexibility in the site regions; more specifically, the binding of a calcium in site II affects the structure and the dynamics of site II and also site I. The binding of a second calcium in site I has a smaller effect on the structure and the dynamics of the protein. Residues Leu23 and Val61, which form a short β-strand with two backbone-backbone hydrogen bonds bridging the two calcium-binding EF-hands, exhibit the smallest rms fluctuations of the entire protein in the D state in accord with *B*-factors.

In all three simulations the calcium(s) remained bound in a stable fashion, although some local alterations were observed in the coordination pattern. The differences in coordination pattern partly reflect the dynamic flexibility of calcium binding sites relative to the average X-ray and NMR structures. However, the neglect of nonadditive induced polarization in the PARAM22 empirical potential function,[35] which plays an important role in ion-peptide interactions,[52,53] may also be an important factor in the deviation from the coordination pattern observe in the X-ray structure. For further quantitative studies, it will be necessary to develop suitable approximations incorporating nonadditive induced polarization effects.

Structural and dynamic factors playing a possible role in calcium binding cooperativity were examined. The two hydrogen bonds between Leu23 and Val61, which give rise to a direct coupling between the two binding sites, are more flexible in the apo state than in the calcium-loaded states. Analysis of average distance maps indicates that there is a larger number of close contacts between the two binding sites in the S_{II} state than in the A state. The importance of van der Waals interactions involving nonpolar side chains in the calcium binding cooperativity was examined. Analysis shows that the interaction of Val61 with the rest of the protein increases progressively with the calcium occupancy (A to S_{II} to D) and appears to favor double occupancy.

Future studies will focus on the energetics of calcium binding cooperativity. To provide a more complete view of the system, the S_I state (singly loaded with the calcium in site I) will be constructed and refined starting from the equilibrated D. The determination of the structure of a half-saturated N56A mutant with calcium in site I is progressing,[70] although it is not yet available. Furthermore, the present calculations indicate that the A state has very large dynamic fluctuations. The structure and dynamics of the A state are currently being explored further using different members in the ensemble of 33 experimentally determined structures given in the Protein Data Base (Tenette and Roux, in preparation). Finally, free energy perturbation simulations will be performed on the four states to estimate the influence of site-directed mutations on the calcium binding cooperativity compared with recent experimental data (S. Linse, personal communication).

ACKNOWLEDGMENTS

B.R. is a MRC research fellow. Useful discussions with C. Tenette are gratefully acknowledged.

REFERENCES

1. Heizmann, C.W., Hunziker, W. Intracellular calcium-binding proteins: More sites than insights. Trends Biochem. Sci. 16:98–103, 1991.
2. Evered, D., Whelan, J., eds. "Calcium and the Cell." New York: John Wiley & Sons, 1986.
3. McPhalen, C.A., Strynadka, N.C., James, M.N. Calcium-binding sites in proteins: A structural perspective. Adv. Protein Chem. 42:77–144, 1991.
4. Strynadka, N.C., James, M.N. Crystal structures of the helix-loop-helix calcium-binding proteins. Annu. Rev. Biochem. 58:951–998, 1989.
5. Strynadka, N.C., James, M.N. Lysozyme revisited: Crystallographic evidence for distortion of an N-acetylmuramic acid residue bound in site D. J. Mole. Biol. 220:401–424, 1991.
6. Ikura, M. Calcium binding and conformational response in EF-hand proteins [Review]. Trends Biochem. Sci. 21:14–17, 1996.
7. Ikura, M., Clore, G.M., Gronenborn, A.M., Zhu, G., Klee, C.B., Bax, A. Solution structure of a calmodulin-target peptide complex by multidimensional NMR. Science 256: 632–638, 1992.
8. Ikura, M., Barbato, G., Klee, C.B., Bax, A. Solution structure of calmodulin and its complex with a myosin light chain kinase fragment. Cell Calcium 13:391–400, 1992.
9. Christakos, N., Gabrielides, C., Rhoten, W. Vitamin D-dependent calcium binding proteins: Chemistry, distribution, functional considerations, and molecular biology. Endocr. Rev. 10:3–26, 1989.
10. Balmain, N. Calbindin D_{9k}, a vitamin D-dependent, calcium-binding protein in mineralized tissues. Clin. Orthop. 265: 265–276, 1991.
11. Linse, S., Brodin, P., Johansson, C., Thulin, E., Grundstrom, T., Forsen, S. The role of protein surface charges in ion binding. Nature 335:651–652, 1988.
12. Linse, S., Johansson, C., Brodin, P., Grundstrom, T., Drakenberg, T., Forsen, S. Electrostatic contributions to the binding of Ca^{2+} in calbindin D_{9k}. Biochemistry 30:154–162, 1991.
13. Kretsinger, R.H., Nockolds, C.E. Carp muscle calcium-binding protein. II. Structure determination and general description. J. Biol. Chem. 248:3313–3326, 1973.
14. Kretsinger, R.H. Calcium-binding proteins. CRC Crit. Rev. Biochem. 8:118–174, 1982.
15. Linse, S., Brodin, P., Drakenberg, T., et al. Structure-function relationships in EF-hand Ca^{2+}-binding proteins. Protein engineering and biophysical studies of calbindin D_{9k}. Biochemistry 26:6723–6735, 1987.
16. Linse, S., Chazin, W.J. Quantitative measurements of the cooperativity in an EF-hand protein with sequential calcium binding. Protein Sci. 4:1038–1044, 1995.
17. Szebenyi, D.M.E., Obendorf, S.K., Moffat, K. Structure of vitamin D-dependent calcium-binding protein from bovine intestine. Nature 294:327–332, 1981.
18. Szebenyi, D.M.E., Moffat, K. The refined structure of vitamin D-dependent calcium-binding protein from bovine intestine. J. Biol. Chem. 261:8761–8777, 1986.

19. Svensson, L.A., Thulin, E., Forsen, S. Proline cis-trans isomers in calbindin D_{9k} observed by X-ray crystallography. J. Mol. Biol. 223:601–606, 1992.
20. Akke, M., Drakenberg, T., Chazin, W.J. Three-dimensional solution structure of $Ca^{(2+)}$-loaded porcine calbindin D9k determined by nuclear magnetic resonance spectroscopy. Biochemistry 31:1011–1020, 1992.
21. Kordel, J., Skelton, N.J., Akke, M., Chazin, W.J. High-resolution structure of calcium-loaded calbindin D_{9k}. J. Mol. Biol. 231:711–734, 1993.
22. Akke, M., Forsen, S., Chazin, W.J. Solution structure of (Cd^{2+})1-calbindin D_{9k} reveals details of the stepwise structural changes along the Apo-¿(Ca^{2+}) II1-¿(Ca^{2+})I,II2 binding pathway. J. Mol. Biol. 252:102–121, 1995.
23. Skelton, N.J., Kordel, J., Chazin, W.J. Determination of the solution structure of Apo calbindin D_{9k} by NMR spectroscopy. J. Mol. Biol. 249:441–462, 1995.
24. Akke, M., Forsen, S., Chazin, W.J. Molecular basis for co-operativity in Ca^{2+} binding to calbindin D9k. ^1H nuclear magnetic resonance studies of (Cd^{2+})1-bovine calbindin D9k. J. Mol. Biol. 220:173–189, 1991.
25. Akke, M., Skelton, N.J., Kordel, J., Palmer, A.G. 3d, Chazin, W.J. Effects of ion binding on the backbone dynamics of calbindin D_{9k} determined by ^{15}N NMR relaxation. Biochemistry 32:9832–9844, 1993.
26. Kordel, J., Skelton, N.J., Akke, M., Palmer, A.G. 3d, Chazin, W.J. Backbone dynamics of calcium-loaded calbindin D_{9k} studied by two-dimensional proton-detected ^{15}N NMR spectroscopy. Biochemistry 31:4856–4866, 1992.
27. Akke, M., Brüschweiler, R., Palmer, A.G. NMR order parameters and free energy: An analytical approach and its application to cooperative Ca^{2+} binding by calbindin D_{9k}. J. Am. Chem. Soc. 115:9832–9833, 1993.
28. Monod, J., Changeux, J.-P., Jacob, F. Allosteric proteins and cellular control systems. J. Mol. Biol. 6:306–329, 1963.
29. Monod, J., Wyman, J., Changeux, J.-P. On the nature of allosteric transitions: A plausible model. J. Mol. Biol. 12:88–118, 1965.
30. Ahlström, P., Teleman, O., Kördel, J., Forsén, S., Jönsson, B. A molecular dynamics simulation of bovine calbindin D_{9k}. Molecular structure and dynamics. Biochemistry 28: 3205–3211, 1989.
31. Kördel, J., Teleman, O. Backbone dynamics of calbindin D_{9k}: Comparison of molecular dynamics simulations and ^{15}N NMR relaxation measurements. J. Am. Chem. Soc. 114:4934–4936, 1992.
32. Mehler, E.L., Kushick, J.N., Weinstein, H. Consequences of sequential Ca^{2+} occupancy for the structure and dynamics of calbindin D_{9k}: Computational simulations and comparison to experimental determinations in solution. Mol. Simulation 10:309–334, 1993.
33. Teleman, O., Jönsson, B. Vectorizing a general purpose molecular dynamics simulation program. J. Comput. Chem. 7:58–66, 1986.
34. Brooks, B.R., Bruccoleri, R.B., Olafson, B.D., States, D.J., Swaminathan, S., Karplus, M. CHARMM: A program for macromolecular energy minimization and dynamics calculations. J. Comput. Chem. 4:187–217, 1983.
35. MacKerrel, et al. All-atom empirical potential for molecular modeling and dynamics studies of proteins. J. Phys. Chem. B 102:3586–3616, 1998.
36. Beglov, D., Roux, B. Finite representation of an infinite bulk system. Solvent boundary potential for computer simulations. J. Chem. Phys. 100:9050–9063, 1994.
37. Marcus, Y. "Ion Solvation." New York: John Wiley & Sons, 1985.
38. Born, M. Volumen und Hydratationswarme der Ionen. Z. Phys. 1:45–48, 1920.
39. Stote, R.H., States, D.J., Karplus, M. On the treatment of electostatic interactions in biomolecular simulation. J. Chim. Phys. 88:2419–2433, 1991.
40. Chazin, W.J., Kordel, J., Drakenberg, T., et al. Proline isomerism leads to multiple folded conformations of calbindin D_{9k}: Direct evidence from two-dimensional ^1H NMR spectroscopy. Proc. Natl. Acad. Sci. USA 86:2195–2198, 1989.
41. Kordel, J., Forsen, S., Drakenberg, T., Chazin, W.J. The rate and structural consequences of proline cis-trans isomerization in calbindin D_{9k}: NMR studies of the minor (cis-Pro43) isoform and the Pro43Gly mutant. Biochemistry 29:4400–4409, 1990.
42. Brunger, A.T., Karplus, M. Polar hydrogen positions in proteins: Empirical energy placement and neutron diffraction comparison. Proteins 4:148–156, 1988.
43. Jorgensen, W.L., Impey, R.W., Chandrasekhar, J., Madura, J.D., Klein, M.L. Comparison of simple potential functions for simulating liquid water. J. Chem. Phys. 79:926–935, 1983.
44. Åqvist, J. Ion water interaction potential derived from free energy perturbation simulations. J. Phys. Chem. 94:8021–8024, 1990.
45. Shimada, J., Kaneko, H., Takada, T. Performance of fast multipole methods for calculating electrostatic interactions in biomacromolecular simulations. J. Comp. Chem. 15:28–43, 1994.
46. Ryckaert, J.P., Ciccotti, G., Berendsen, H.J.C. Numerical integration of the cartesian equation of motions of a system with constraints: Molecular dynamics of *n*-alkanes. J. Comp. Chem. 23:327–341, 1977.
47. Kollman, P.A. Free Energy Calculations: Applications to Chemical and Biochemical Phenomena. Chem. Rev. 93: 2395–2417, 1993.
48. Frisch, M.J., Head-Gordon, M., Trucks, G.W., et al. "Gaussian 90." Pittsburgh, PA: Gaussian Inc., 1990.
49. Wachters, A.J.H. Gaussian basis set for molecular wave functions containing third row atoms. J. Chem. Phys. 52:1033–1036, 1970.
50. Gianolo, L., Pavani, R., Clementi, E. A new algorithm for obtaining contracted basis sets from gaussian type function. Gazzetta Chim. Ital. 108:181–205, 1978.
51. Boys, S.F., Bernardi, F. The calculation of small molecular interactions by the differences of separate total energies. Some procedures with reduced errors. Mol. Phys. 19:553–566, 1970.
52. Roux, B. Nonadditivity in cation-peptide interactions: A molecular dynamics and ab initio study of Na^+ in the gramicidin channel. Chem. Phys. Lett. 212:231–240, 1993.
53. Woolf, T.B., Roux, B. The binding site of sodium in the gramicidin A channel: A comparison of molecular dynamics simulations with solid state NMR data. Biophys. J. 72:1930–1945, 1997.
54. Lee, B., Richards, F.M. The interpretation of protein structures: Estimation of static accessibility. J. Mol. Biol. 55:379–400, 1971.
55. Willis, B.T.M., Pryor, A.W. "Thermal Vibrations in Crystallography." Cambridge: Cambridge University Press, 1975.
56. Clore, G.M., Szabo, A., Bax, A., Kay, L., Driscoll, P.C., Gronenborn, A.M. Deviations from the simple two-parameter model-free approach to the interpretation of nitrogen-15 nuclear magnetic relaxation of proteins. J. Am. Chem. Soci. 112:4989–4991, 1990.
57. Clore, G.M., Driscoll, P.C., Wingfield, P.T., Gronenborn, A.M. Analysis of the backbone dynamics of interleukin-1β using two-dimensional inverse detected heteronuclear ^{15}N-^1H NMR spectroscopy. Biochemistry 29:7387–7401, 1990.
58. Brüshweiler, R., Roux, B., Blackledge, M., Griesinger, C., Karplus, M., Ernst, R.R. Influence of rapid intramolecular motion on NMR cross-relaxation rates. A molecular dynamics study of antamanide in solution. J. Am. Chem. Soc. 114:2289–2302, 1992.
59. Abragam, A. "Principles of Nuclear Magnetism." Oxford: Oxford University Press, 1961.
60. Ernst, R.R., Bodenhausen, G., Wokaun, A. "Principle of NMR in One and Two Dimensions. Oxford: Clarendon Press, 1987.
61. Lipari, G., Szabo, A. Model-free approach to the interpretation of nuclear magnetic resonance relaxation in macromol-

ecules. 1. Theory and range of validity. J. Am. Chem. Soc. 104:4546–4559, 1982.
62. Smith, L.J., Mark, A.E., Dobson, C.M., van Gunsteren, W.F. Comparison of MD simulations and NMR experiments for hen lysozyme. Analysis of local fluctuations, cooperative motions, and global changes. Biochemistry 34:10918–10923, 1995.
63. Li, Z., Raychaudhuri, S., Wand, A.J. Insights into the local residual entropy of proteins provided by NMR relaation. Protein Sci. 5:2647–2650, 1996.
64. Yang, D., Kay, L.E. Contributions to conformational entropy arising from bond vector fluctuations measured from NMR-derived order parameters: Application to protein folding. J. Mol. Biol. 263:369–382, 1996.
65. Chandrasekhar, I., Clore, G.M., Szabo, A., Gronenborn, A.M., Brooks, B.R. A 500 ps molecular dynamics simulation study of interleukin-1β in water. J. Mol. Biol. 226:239–250, 1992.
66. Eriksson, M.A.L., Berglund, H., Härd, T., Nilsson, L. A comparison of ^{15}N-NMR relaxation measurements with a molecular dynamics simulation: Backbone dynamics of the glucocorticoid receptor DNA-binding domain. Proteins 17: 375–390, 1993.
67. Smith, P.E., van Schaik, R.C., Szyperski, T., Wütrich, K., van Gunsteren, W.F. Internal mobility of the basic pancreatic trypsin inhibitor in solution: A comparison of NMR spin relaxation measurements and molecular dynamics simulations. J. Mol. Biol. 246:356–365, 1995.
68. Yamasaki, K., Minoru, S., Oobatake, M., Kanaya, S. Characterization of the internal motions of *Escherichia coli* ribonuclease H_1 by a combination of ^{15}N-NMR relaxation analysis and molecular dynamics simulation: Examination of dynamic models. Biochemistry 34:6587–6601, 1995.
69. Philippopoulos, M., Lim, C. Molecular dynamics simulation of *E. coli* ribonuclease H_1 in solution: Correlation with NMR and X-ray data and insights into biological function. J. Mol. Biol. 254:771–792, 1995.
70. Wimberly, B., Thulin, E., Chazin, W.J. Characterization of the N-terminal half-saturated state of calbindin D_{9k}: NMR studies of the N56A mutant. Protein Sci. 4:1045–1055, 1995.